Journal of Alloys and Compounds 495 (2010) 189–195

Contents lists available at ScienceDirect

Journal of Alloys and Compounds

journal homepage: www.elsevier.com/locate/jallcom

# Microstructure characteristic and excellent corrosion protection properties of sealed Zn–$TiO_2$ composite coating for sintered NdFeB magnet

Xiaokui Yang [b], Qing Li [a,*], Shiyan Zhang [a], Fang Liu [a], Shaoyin Wang [a], Haixiao Zhang [a]

[a] School of Chemistry and Chemical Engineering, Southwest University, Chongqing 400715, PR China
[b] School of Materials Science and Engineering, Southwest University, Chongqing 400715, PR China

ARTICLE INFO

*Article history:*
Received 28 December 2009
Received in revised form 18 January 2010
Accepted 21 January 2010
Available online 1 February 2010

*Keywords:*
NdFeB permanent magnet
Zn–$TiO_2$
Corrosion protection
Sealing

ABSTRACT

In this paper, a protective sealed Zn–$TiO_2$ composite coating (SCC) was prepared on sintered NdFeB magnet by electrodeposition and sol–gel combined technique. For a comparison, unsealed Zn–$TiO_2$ composite coating (UCC) was also studied. The surface morphologies of composite coating were studied using scanning electron microscope (SEM). The microstructure of composite coatings and structure of sealing layer were studied by X-ray diffraction (XRD) and Fourier transform infrared (FT-IR) spectrum, respectively. The anticorrosive properties of composite coatings in neutral 3.5 wt.% NaCl solutions were evaluated by potentiodynamic polarization and electrochemical impedance spectroscopy (EIS) technique. The results of corrosion tests showed that due to the blocking effect of sealing layer, SCC could suppress the corrosion process by holding back the transfer or diffusion of corrosive medium, and therefore showed the excellent corrosion protection properties for sintered NdFeB magnet.



## 1. Introduction

The sintered NdFeB (neodymium–iron–boron) magnet, which was developed at the beginning of the 1980s, has been used for many applications in various fields such as acoustics, communications, and automation due to its excellent properties such as high remanence, high coercivity, and large energy product [1–3]. However, sintered NdFeB permanent magnet is highly vulnerable to the attack of corrosive environment, which impedes and limits their extensive applications [4,5].

In order to improve the corrosion resistance of sintered NdFeB magnet, numerous attempts have been made, such as alloy additions and surface treatment [6–17], among which the electroplating of metal coatings is one of the most popular methods [10,13–17]. Within our knowledge, most of the coatings on the sintered NdFeB magnet are cathodic coatings [10,13–17], and seldom of the anodic coating [8]. As is well known, the main role of cathodic coating in the corrosion protection for sintered NdFeB magnet is mechanical isolation, which could segregate the sintered NdFeB magnet with corrosive media. Once the cathodic coating suffers physical deterioration and electrochemical corrosion, which may result in the exposition of sintered NdFeB magnet to corrosive media in some sites, the phenomenon that bigger cathode versus smaller anode occurs, which could accelerate the corrosion of sintered NdFeB magnet. The role of anodic coating in corrosion protection for metal substrate is a combination of mechanical isolation and electrochemical protection. Though anodic coating suffers physical deterioration and electrochemical corrosion, which could conduce to the exposition of metal substrate to corrosive media in some sites, the anodic coating may act as sacrificial anode and slower the corrosion of metal substrate [18].

Among all surface coatings, zinc coatings may be one of most promising and potential anodic coating due to its low cost and maneuverability [19]. With the development of scientific technology, the pure zinc coatings cannot satisfy the requirements of industrial applications, and it leads to the high requirement of properties of coatings. The electrodeposition of zinc matrix composite coatings containing nano-particles on mild steel, stainless steel, copper and aluminum, etc., which exhibit excellent properties including higher wear and corrosion resistance, higher hardness, more excellent self-lubricating in comparison with single zinc coatings, have been widely studied [20–22]. However, electrodeposited zinc matrix composite coatings on sintered NdFeB permanent magnet have not yet been reported.

In the present work, electrodeposited Zn–$TiO_2$ composite coating was successfully performed on sintered NdFeB magnet. The most adopted method for the further enhancement on the anticorrosive properties of zinc coatings is chromating which is harmful to environments and health. In order to further improve the anticorrosive properties of Zn–$TiO_2$ composite coating, an environmentally friendly sealing method had been developed. The effectiveness of sealed Zn–$TiO_2$ composite coating on corrosion protection

* Corresponding author. Tel.: +86 023 68252360; fax: +86 023 68367675.
*E-mail addresses:* liqingd@swu.edu.cn, woshihai@swu.edu.cn (Q. Li).

0925-8388/$ – see front matter © 2010 Elsevier B.V. All rights reserved.
doi:10.1016/j.jallcom.2010.01.117

**Table 1**
Chemical compositions of experimental sintered NdFeB magnet.

| | Element | | | | | | | | |
|---|---|---|---|---|---|---|---|---|---|
| | Fe | Nd | B | Dy | Al | Co | Si | Cu | Nb |
| wt.% | 60.9 | 28.6 | 1.0 | 2.1 | 3.8 | 1.3 | 1.4 | 0.2 | 0.7 |
| at.% | 67.9 | 12.3 | 5.8 | 0.8 | 8.1 | 1.4 | 3.1 | 0.2 | 0.4 |

properties for sintered NdFeB magnet was evaluated by potentiodynamic polarization and electrochemical impedance spectroscopy (EIS). The main aim of this study is to attempt the electrodeposition of anodic coating on sintered NdFeB magnet, and introduce the environmentally friendly sol–gel method to slower the corrosion rate of anodic coating. The anticorrosive properties of sealed Zn–$TiO_2$ composite coating were investigated in neutral 3.5 wt.% NaCl solutions which are the most adopted corrosive media, suggesting the feasibility of the long-term corrosion protection for NdFeB magnet.

## 2. Experimental details

### 2.1. Materials

The commercial powder-sintered NdFeB magnet for this investigation was purchased from Shenzhen (Dongsheng Magn. Mater. Co., Ltd., China). They were in disk form with diameter and thickness of 12.0 mm and 2.0 mm, respectively. The chemical compositions of sintered NdFeB magnet are listed in Table 1. The zinc plate was used as anode on both sides of the electrolytic cell.

### 2.2. Pretreatment of magnet

Before electrodeposition, the disc NdFeB magnet (substrate) was sequentially polished with silicon carbide paper from grit #400 to #2000, rinsed with deionized water, ultrasonically degreased in an alkaline solutions containing 70 g $L^{-1}$ $Na_3PO_4{\cdot}12H_2O$, 50 g $L^{-1}$ $Na_2CO_3$, 10 g $L^{-1}$ NaOH, 0.5 g $L^{-1}$ sodium dodecyl sulfate (SDS) and 0.5 g $L^{-1}$ OP-10 (pH adjusted to 10–11 by formic acid) at 70 °C for 2 min and then rinsed with hot and cold deionized water, respectively. In order to remove the oxide film on the surface of NdFeB magnet, the above pretreated NdFeB magnet was dipped into an acid solutions containing 40 mL $L^{-1}$ $HNO_3$ (65.0 wt.%) and 0.5 g $L^{-1}$ thiourea with the pH adjusted to 4–5 by ammonia, for approximately 10 s at room temperature. At last, the NdFeB magnet was activated by the anhydrous $PdCl_2$/EtOH solutions, with the $PdCl_2$ of 0.4 g $L^{-1}$, for 2–5 s at room temperature.

### 2.3. Electrodeposition process

The optimized bath composition and other parameters for the electrodeposition of Zn–$TiO_2$ composite coating, which were obtained from large numbers of orthogonal experiments, are given in Table 2.

### 2.4. Synthesis of sealing agent and sealing process

The sealing agent was silane sol (Si sol) which was prepared using the following two-step process (i) acid catalysis-based hydrolysis and (ii) alkaline catalysis-based condensation. Acetic acid (pH < 6) was initially introduced into the stirring mixture including tetraethyl orthosilicate (TEOS) and triethoxyvinylsilane (VTEO) (1.16 mol/L Si in ethanol and TEOS:VTEO in a 1:3 molar ratio) drop by drop at 60 °C, then stirred for 30 min, and then ammonia was introduced into the mixed solution drop by drop until the pH of the precursor was 7.0. Finally, the formed silane sol (Si sol) was aged for 1 day at room temperature before deposition on the Zn–$TiO_2$ composite coating.

**Table 2**
Bath compositions and operating conditions for electrodeposition.

| Bath compositions and operating conditions | Quantity |
|---|---|
| $ZnCl_2$ | 40 g $L^{-1}$ |
| $NH_4Cl$ | 250 g $L^{-1}$ |
| $CH_3COOH$ (≥99.5%) | 100 mL $L^{-1}$ |
| $SC(NH_2)_2$ | 1.5 g $L^{-1}$ |
| $TiO_2$ | 10 g $L^{-1}$ |
| SDS | 0.2 g $L^{-1}$ |
| Current density | 4 A $dm^{-2}$ |
| pH | 4 |
| Temperature | 25 °C |
| Time | 30 min |
| Agitation | Continuous |

The silane sol (Si sol) was employed as sealing agent, and the method of sealing was dip-coating technique. After immersion in the sealing agent for about 3 min, the specimens were taken out and cured in an oven at 100 °C for 60 min [13]. The process mentioned above was cycled twice.

### 2.5. Tests

The surface morphologies and compositions of coatings were studied using a scanning electron microscope (SEM) (Model TESCAN VEGAIILMU, Czech) coupled with energy dispersive analyzer system (EDS). In each EDS measurement, an area of 10 μm in diameter is examined to a depth of about 2 μm, and the EDS measurement was repeated three times at least.

The phase structures of coatings were analyzed by X-ray diffractometer (XRD) (Beijing Purkinje general instrument Co., Ltd., China) operated at 36 kV and 20 mA with Cu $K_a$ radiation. The average crystallite size was determined using Scherrer equation.

The Fourier transform infrared (FT-IR) spectrum recorded with an IR-10300 (TENSOR-27, Germany) was carried out to analyze the structure of silane sol (Si sol).

The coating adhesion was evaluated according to ASTMB571 standard (heat quenching test, 220 °C aging treatment for 1 h, then water quenching at room temperature).

The electrochemical corrosion tests were carried out using a classical three electrodes cell with platinum as counter electrode, saturated calomel electrode SCE (+0.242 V vs. SHE) as reference electrode, and the samples with an exposed area of 1 $cm^2$ as working electrode. The potentiodynamic polarization curves were performed by PS-268B system (Zhongfu, Beijing, China) with a constant voltage scan rate of 0.5 mV $s^{-1}$. The electrochemical impedance spectroscopy (EIS) measurements were performed with CS350 electrochemical workstation (Wuhan CorroTest Instrument Co., Ltd., China). The amplitude of sinusoidal signal employed was 5 mV, and the frequency range studied was from $10^5$ to $10^{-2}$ Hz. The acquired data were curve fitted and analyzed using *ZsimpWin 3.10* software. The corrosive media used for electrochemical corrosion tests were neutral 3.5 wt.% NaCl solutions, and the test temperature was maintained 25 °C. All the electrochemical corrosion tests were normally repeated at least three times under the same conditions, checking that they presented reasonable reproducibility.

## 3. Results and discussion

### 3.1. SEM analysis

The surface morphologies of sealed composite coating (SCC) and unsealed composite coating (UCC) are shown in Fig. 1. Fig. 1a showed that UCC was compact and presented regular samdwich.

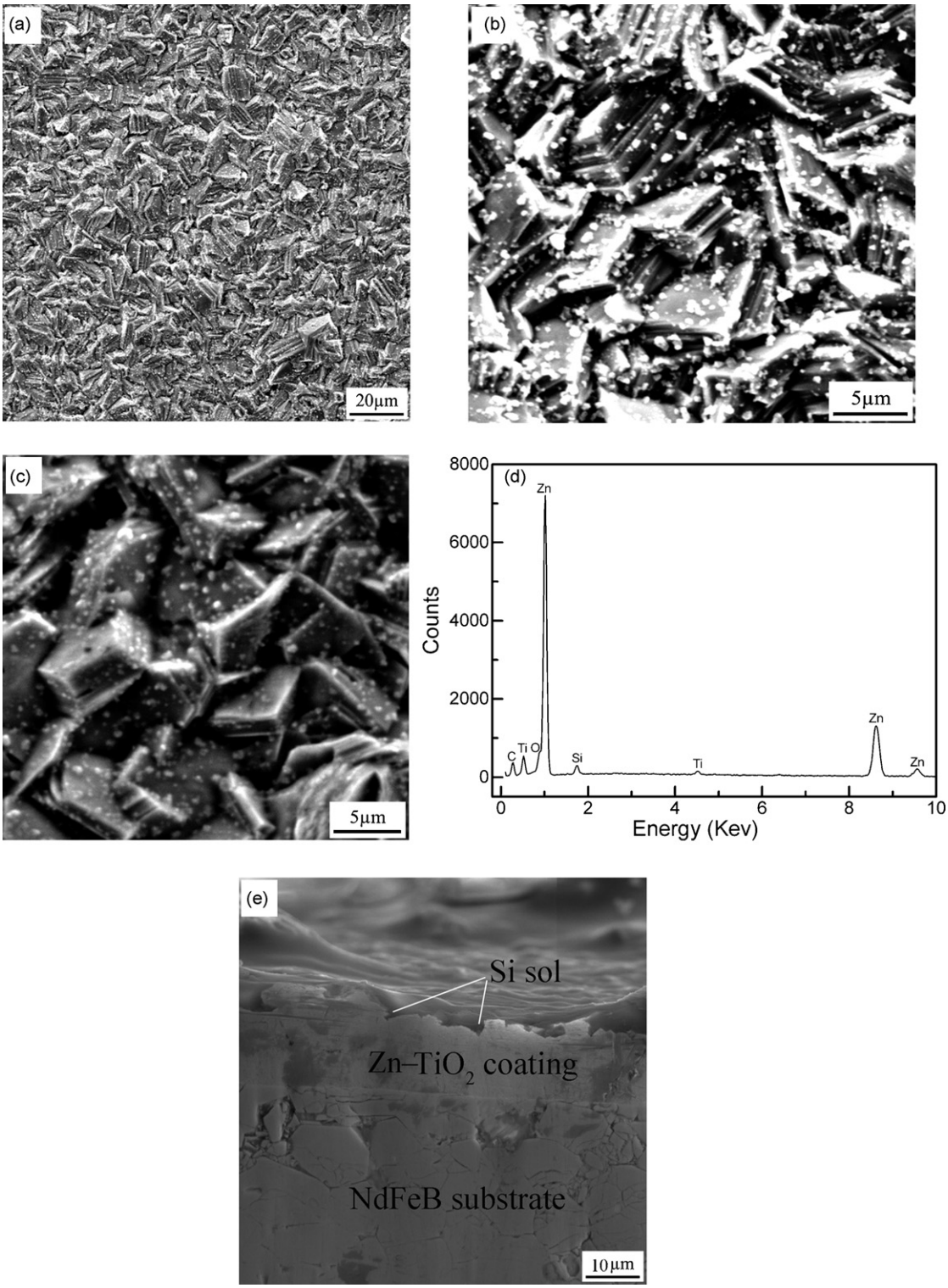


**Fig. 1.** Surface morphologies of UCC (a and b), SCC (c), EDS spectrum of SCC (d) and cross-section morphologies of SCC (e).

The EDS results revealed that the content of $TiO_2$ was $1.1 \pm 0.1$ wt.%. A magnified scanning electron micrograph for UCC is presented in Fig. 1b. It can be seen that the samdwich was more obvious and some white particles were observed. The EDS analysis showed that the content of $TiO_2$ for white particles was higher than the other area, suggesting that they were the fresh deposits enriched with the $TiO_2$ particles, while in the other areas the codeposited $TiO_2$ particles were engulfed by Zn deposits [23]. The surface morphology of SCC with a high magnification is shown in Fig. 1c. There was no obvious difference in structure between Fig. 1b and c due to the transparence of the Si sol. The EDS revealed the existence of Si sol (Fig. 1d). According to the adhesion test, the phenomena of blisters and crackles were not found. Thus, the adhesion between UCC and the NdFeB substrate was good. From the cross-section morphologies, as shown in Fig. 1e, it can be seen that the thickness of SCC was $14 \pm 2$ μm.

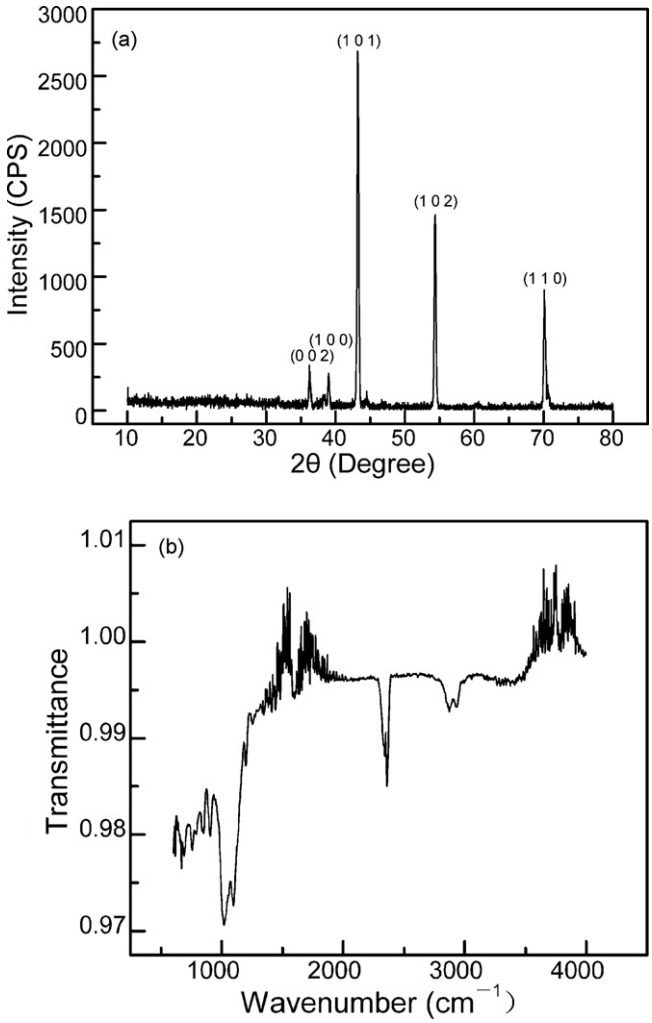


**Fig. 2.** X-ray diffraction patterns of UCC (a) and FT-IR spectrum of SCC (b).

### 3.2. Microstructure analysis

The XRD pattern of unseal Zn–$TiO_2$ composite coating (UCC) is shown in Fig. 2a. Fig. 2a showed that the XRD pattern of UCC exhibited five acute peaks centered 2$\theta$ at 36.290°, 38.995°, 43.221°, 54.322° and 70.633° corresponding to Zn (0 0 2), (1 0 0), (1 0 1), (1 0 2) and (1 1 0) phase, respectively, indicating the crystal nature of the composite coatings. The average grain size of UCC was 45 nm. The characteristic peak of $TiO_2$ in composite coating was not observed in the XRD patterns perhaps owing to the little content in composite coatings. However, the EDS analysis testified the existence of $TiO_2$ particles in composite coating which was analyzed in SEM analysis.

The FT-IR absorption spectrum of SCC is shown in Fig. 2b. It is known that the Si–O–Si has an asymmetric stretching mode in a wide region [24], and the location depends upon the nature of the bonding associated with it. In Fig. 2b, an obvious absorption peak presented at around 1106 cm$^{-1}$, which was attributed to $\nu_{as}$(Si–O–Si), was observed. The absorption peak of $CO_2$ was observed at 2368 cm$^{-1}$ due to the non-flat surface of SCC.

### 3.3. Potentiodynamic polarization analysis

The typical potentiodynamic polarization curves of the different specimens are presented in Fig. 3.

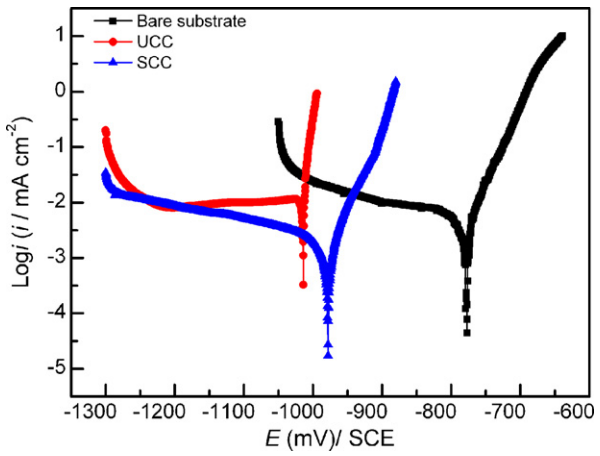


**Fig. 3.** Typical potentiodynamic polarization curves of different specimens in neutral 3.5 wt.% NaCl solutions.

Fig. 3 showed that bare substrate, UCC and SCC all exhibited active dissolution without any distinctive transition to passivation within the range of anodic potential studied. With the increasing anodic potential, the anodic current densities significantly increased for three specimens, suggesting a fast anodic dissolution.

Different parameters like corrosion current density ($i_{corr}$) and corrosion potential ($E_{corr}$), cathodic ($\beta_c$) and anodic ($\beta_a$) Tafel slopes derived from Fig. 3 using Tafel extrapolation are summarized in Table 3. It can be seen that the $E_{corr}$ of bare substrate was higher than that of both UCC and SCC, indicating that both UCC and SCC can act as anodic coatings to play the role of mechanical isolation and electrochemical protection in the corrosion protection for sintered NdFeB magnet. Comparing UCC with SCC, it can be found that the value of $i_{corr}$ for SCC was near upon two orders of magnitude lower than that of $i_{corr}$ for UCC, suggesting the lower corrosion rate for SCC. Furthermore, the value of $E_{corr}$ for SCC was slightly nobler than that of $E_{corr}$ for UCC, indicating the higher thermodynamics stability for SCC. In addition, the UCC presented the rather low anodic Tafel slope (1.3 mV/decade), suggesting the fast active dissolution during polarization in 3.5% NaCl solutions. The anodic Tafel slope of SCC (38.72 mV/decade) markedly increased due to the blocking effect of the sealing layer.

The different polarization behavior for SCC and UCC was mainly due to their different properties and structure. As to SCC, due to the covering and blocking effect of sealing layer, transfer of corrosive media was held back to a certain extent and the increase of polarization current was suppressed during polarization treatment. Consequently, the corrosion process of SCC was slowed down, i.e. the anodic portion of the polarization curve of SCC showed the lower anodic current densities and higher anodic ($\beta_a$) Tafel slopes.

### 3.4. Electrochemical impedance spectroscopy analysis

Electrochemical impedance spectroscopy (EIS) is one of the most intensively used and powerful techniques for investigation and prediction of corrosion protection [25].

The typical EIS plots displayed in Figs. 4 and 5 clearly showed the distinct differences among the different specimens. From Fig. 4 (impedance modulus $|Z|$ as a function of frequency), it can be seen that the impedance value of SCC coated substrate increased by approximately one order of magnitude compared with that of UCC coated substrate, indicating that the SCC possessed the higher corrosion resistance compared with UCC. Fig. 4 (phase angle as a function of frequency) indicates that there was two time constants over the whole frequency range studied for the bare substrate. The appearance of the time constant at high-frequency

**Table 3**
Electrochemical parameters calculated from the potentiodynamic polarization curves displayed in Fig. 3.

| Specimens | $E_{corr}$ (mV vs. SCE) | $I_{corr}$ (A cm$^{-2}$) | $\beta_a$ (mV/decade) | $\beta_c$ (mV/decade) | $R_p$ (Ω cm$^2$) |
|---|---|---|---|---|---|
| SCC | −977.9 | $3.1 \times 10^{-6}$ | 38.72 | 133.34 | 6915 |
| UCC | −1014.1 | $1.9 \times 10^{-4}$ | 1.3 | −861.564 | 114 |
| Substrate | −776.5 | $1.1 \times 10^{-5}$ | 37 | 148 | 1937 |

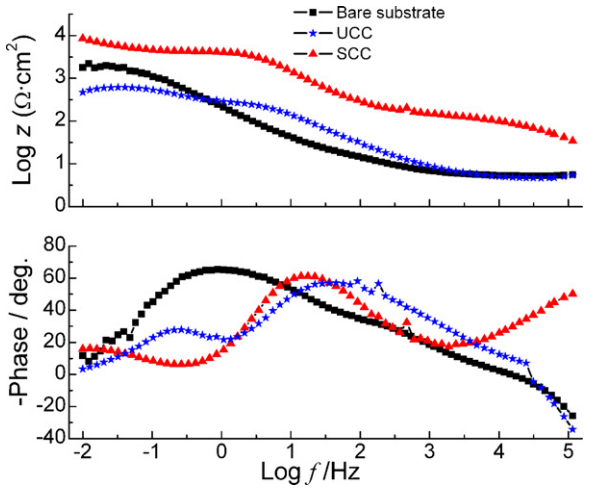


**Fig. 4.** Typical Bode plots of different specimens in neutral 3.5 wt.% NaCl solutions.

range could be attributed to the existence of the corrosion product layer, and the present of the time constant in low-frequency range was attributed to Faradaic reactions of NdFeB magnet. The Nyquist plot of the UCC coated substrate consisted of a high-frequency capacitive loop, intermediate-frequency capacitive loop and a low-frequency inductive loop. The capacitive loop in high-frequency range could be attributed to the existence the corrosion product layer, and the capacitive loop in intermediate-frequency range could be attributed to Faradaic reactions of Zn–$TiO_2$ composite coating. The appearance of low-frequency inductive loop may be ascribed to activated adsorption of intermediate on the surface of electrode [25]. The shape of the phase angle plot and Nyquist plot (Figs. 4 and 5) of SCC coated substrate indicated the existence of three time constants which reflected three relaxation processes. The time constant in high-frequency range was associated with the existence of a protective sealing layer. Due to the blocking effect of sealing layer, the electrochemical corrosion action could be inhibited and then the formation of the corrosion product layer became difficulty, so it is still worthwhile to discuss the origin of relaxation process in the intermediate-frequency range. Van Ooij's [26] and other group [27] who had studied the silane films on aluminum proposed that this time constant was attributed to the chemical formation of an "interfacial inorganic layer" between aluminum base and up-coated silane films. This layer may be composed of natural aluminum oxide and (or) Al–O–Si bonds. The Me–O–Si (Me stands for metals) structure had been detected in many silane-covered metals surface [28,29]. In the present case, the origin of relaxation process in the intermediate-frequency range may be ascribed to existence of combination of the interfacial inorganic layer and some corrosion product according to the studies mentioned above [26–29]. The third one in low-frequency range could be attributed to the existence of Zn–$TiO_2$ composite coating.

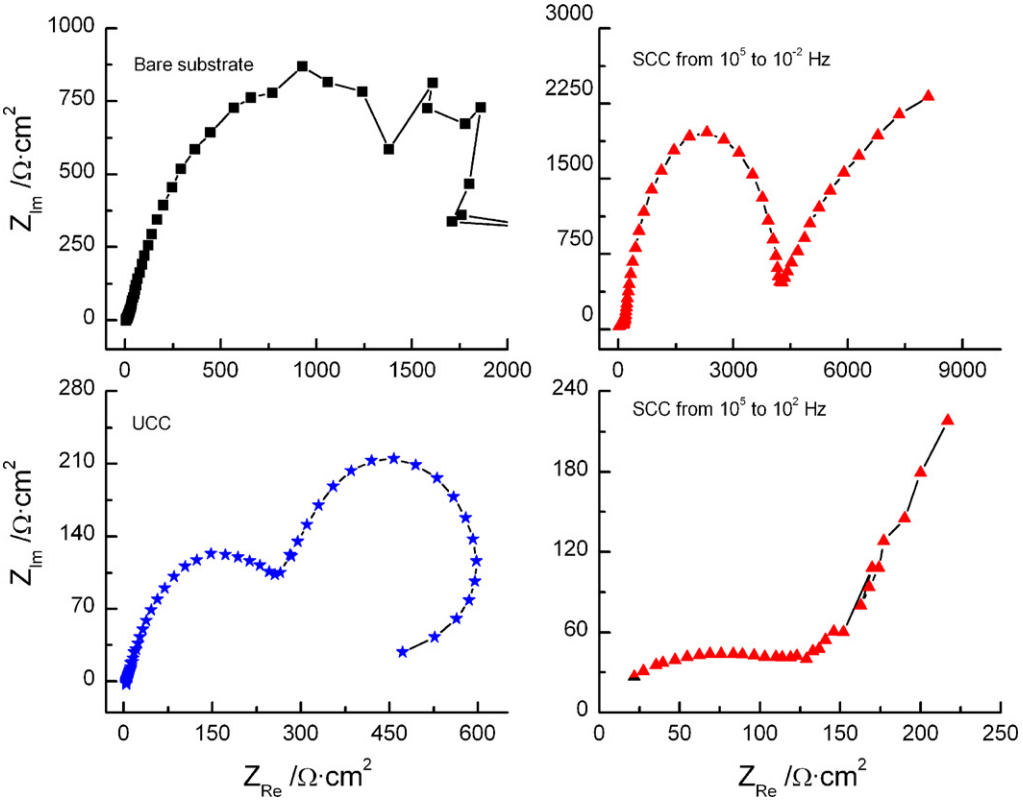


**Fig. 5.** Typical Nyquist plots of different specimens in neutral 3.5 wt.% NaCl solutions.

**Table 4**
Electrochemical equivalent circuit parameters for the different samples.

| Specimens | $R_{si}$ ($\Omega$ cm$^2$) | $Y_0$ ($\Omega^{-1}$ cm$^{-2}$ s$^{-n}$) | $n$ | $R_{mix}$ ($\Omega$ cm$^2$) | $Y_0$ ($\Omega^{-1}$ cm$^{-2}$ s$^{-n}$) | $n$ | $R_{ct}$ ($\Omega$ cm$^2$) | $Y_0$ ($\Omega^{-1}$ cm$^{-2}$ s$^{-n}$) | $n$ |
|---|---|---|---|---|---|---|---|---|---|
| SCC | 170.3 | $4.6 \times 10^{-6}$ | 0.64 | 4515 | $1.3. \times 10^{-5}$ | 0.90 | 4047 | $2.5 \times 10^{-3}$ | 1.0 |

| Specimens | $R_{cor}$ ($\Omega$ cm$^2$) | $Y_0$ ($\Omega^{-1}$ cm$^{-2}$ s$^{-n}$) | $n$ | $R_{ct}$ ($\Omega$ cm$^2$) | $Y_0$ ($\Omega^{-1}$ cm$^{-2}$ s$^{-n}$) | $n$ | $L$ (H cm$^2$) |
|---|---|---|---|---|---|---|---|
| UCC | 346.5 | $2.6 \times 10^{-4}$ | 0.75 | 278.8 | $4.5 \times 10^{-3}$ | 1.0 | 98.9 |
| Substrate | 21.0 | $3.1 \times 10^{-4}$ | 0.83 | 2177 | $6.6 \times 10^{-4}$ | 0.83 | |

A more detailed interpretation of EIS measurement was performed by fitting the experimental plots using the electrochemical equivalent circuit (EEC) depicted in Fig. 6. The EEC displayed in Fig. 6a was proposed to account for the EIS data of bare substrate, while the EEC presented in Fig. 6b and c, were used for the illumination of the UCC coated substrate and SCC coated substrate, respectively. The equivalent circuit presented in Fig. 6a consisted of parameters, namely, solution resistance ($R_s$), the resistance of corrosion product ($R_{cor}$), the charge transfer resistance ($R_{ct}$). The constant phase element (*CPE*) was introduced in order to replace the capacitance of the double layer ($C_{dl}$). A constant phase element (*CPE*) replaced the capacitance of the double layer ($C_{dl}$) due to the roughness and inhomogeneity of the electrode surface as reported elsewhere [25,30]. The impedance of *CPE* was given by the following equation [25]:

$$Z_{CPE}(\omega) = Y_0^{-1}(j\omega)^{-n} \quad (1)$$

where $Y_0$ is a constant that is independent of frequency, $\omega$ is angular frequency, $j = \sqrt{-1}$ and $n$ is exponential index which represents a dispersion of relaxation. The CPE represents a capacitor for $n = 1$, a resistor for $n = 0$, an inductance for $n = -1$ and a diffusion process for $n = 0.5$. The circuit, presented in Fig. 6b, consisted of two *RC* circuits. The circuit $R_{cor}CPE_1$ indicated the corrosion resistance of corrosion product layer corresponding to the high-frequency range of impedance spectroscopy, and $R_{ct}CPE_2$ described the electrode Faraday process, i.e. dissolution of Zn–$TiO_2$ composite coating corresponding to the low-frequency range of impedance spectroscopy. An inductance was introduced to explain the inductive loop in low-frequency range of the measured impedance spectra. The circuit presented in Fig. 6c consisted of three *RC* circuits. The circuit $R_{si}CPE_1$ indicated the corrosion resistance of sealing layer corresponding to the high-frequency range of impedance spectroscopy.

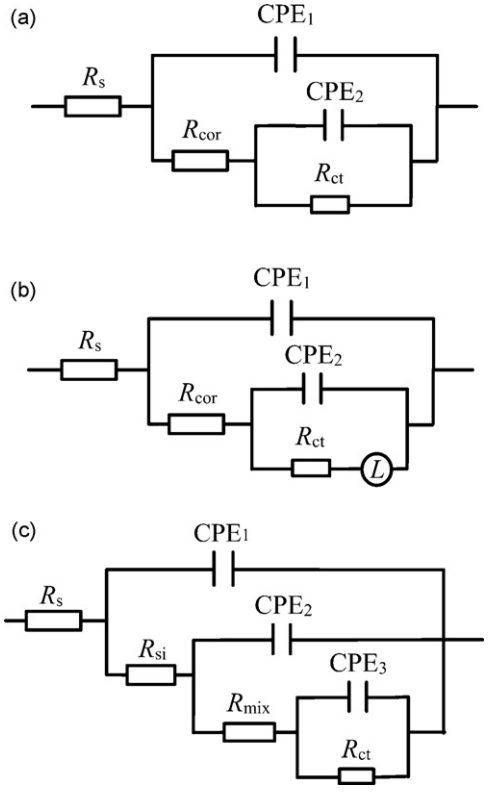


**Fig. 6.** Electrochemical equivalent circuits used for fitting the EIS data of bare substrate (a), UCC coated substrate (b) and SCC coated substrate (c).

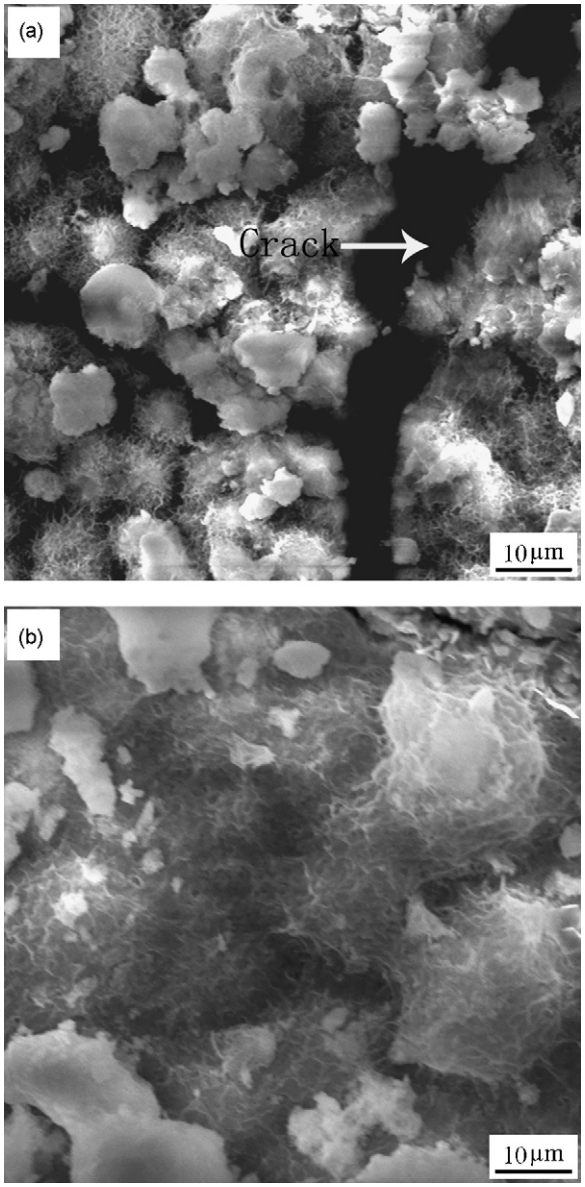


**Fig. 7.** Surface morphologies of the UCC coated substrate (a) with an immersion time of 264 h and SCC coated substrate (b) with an immersion time of 336 h in neutral 3.5 wt.% NaCl solutions.

The circuit $R_{mix}CPE_2$ represented the existence of combination of interfacial layer and corrosion product corresponding to the intermediate-frequency range of impedance spectroscopy, and $R_{ct}CPE_3$ described the electrode Faraday process, i.e. dissolution of Zn–$TiO_2$ composite coating corresponding to the low-frequency range of impedance spectroscopy. The values of the main electrochemical equivalent circuit parameters for different samples are shown in Table 4. From Table 4 it is found that the $R_{ct}$ of SCC with a value of 4047 Ω $cm^2$, were approximately 15 times higher than that of UCC with a value of 278 Ω $cm^2$, which suggested the better anticorrosive properties of SCC than that of UCC.

Fig. 7 showed the surface morphologies of the UCC coated substrate with an immersion time of 264 h and SCC coated substrate with an immersion time of 336 h in neutral 3.5 wt.% NaCl solutions. Large number of corrosion spots and corrosion products were noticed on the SEM image of UCC coated substrate (Fig. 7a). Very little corrosion was observed on the surface of SCC coated substrate (Fig. 7b), which indicated that the degree of corrosion for SCC was much lower than that of UCC. Moreover, the obvious phenomena of crack for UCC were observed. Macroscopic pitting on the surface of SCC coated substrate and the brown rust in solutions cannot be observed with an immersion time of 336 h, but the macroscopic pitting on the surface of UCC coated substrate and the brown rust in solutions were observed when the immersion time was 264 h, suggesting the better corrosion protection properties of the SCC provided for NdFeB magnet in neutral 3.5 wt.% NaCl solutions compared with UCC.

From the corrosion analysis mentioned above, it can be seen that the sealed Zn–$TiO_2$ composite coating (SCC) exhibited excellent anticorrosive properties. Due to the blocking effect of sealing agent [31], SCC could provide better corrosion protection for NdFeB magnet compared with UCC in neutral 3.5 wt.% NaCl solutions.

## 4. Conclusions

A sealed Zn–$TiO_2$ composite coating (SCC), which exhibited excellent corrosion protection properties, was successfully applied to sintered NdFeB magnet by the combination of electrodeposition and the sol–gel method.

The electrochemical corrosion tests indicated that, in comparison to unsealed Zn–$TiO_2$ composite coating (UCC), sealed Zn–$TiO_2$ composite coating (SCC) exhibited better anticorrosive properties, and could provide long-term corrosion protection for NdFeB magnet in neutral 3.5 wt.% NaCl solutions which could be attributed to the blocking effect of sealing agent.

## Acknowledgments

The authors acknowledge with thanks the financial supports granted by the Natural Science Foundation of Chongqing, China (CSTC. 2005BB4055), and the High-Tech Cultivation Program of Southwest Normal University (No. XSGX06).

## References

[1] Y. Matsuura, J. Magn. Magn. Mater. 303 (2006) 344–347.
[2] G. Bai, R.W. Gao, Y. Sun, G.B. Han, B. Wang, J. Magn. Magn. Mater. 308 (2007) 20–23.
[3] F. Vial, F. Joly, E. Nevalainen, M. Sagawa, K. Hiraga, K.T. Park, J. Magn. Magn. Mater. 242–245 (2002) 1329–1334.
[4] D.F. Cygan, M.J. McNallanm, J. Magn. Magn. Mater. 139 (1995) 131–138.
[5] M. Rada, A. Gebert, I. Mazilu, K. Khlopkov, O. Gutfleisch, L. Schultz, W. Rodewald, J. Alloys Compd. 415 (2006) 111–120.
[6] A. Saliba-Silva, R.N. Faria, M.A. Baker, I. Costa, Surf. Coat. Technol. 185 (2004) 321–328.
[7] S. Sunada, K. Majima, Y. Akasofu, Y. Kaneko, J. Alloys Compd. 408–412 (2006) 1373–1376.
[8] K. Majima, S. Sunada, H. Ito, Y. Kaneko, J. Alloys Compd. 408–412 (2006) 1426–1428.
[9] A. Walton, J.D. Speight, A.J. Williams, I.R. Harris, J. Alloys Compd. 306 (2000) 253–261.
[10] C.W. Cheng, F.T. Cheng, J. Appl. Phys. 83 (1998) 6417–6419.
[11] S.M. Tamborim Takeuchi, D.S. Azambuja, I. Costa, Surf. Coat. Technol. 201 (2006) 3670–3675.
[12] L. Song, Y. Wang, W. Lin, Q. Liu, Surf. Coat. Technol. 202 (2008) 5146–5150.
[13] X.K. Yang, Q. Li, J.Y. Hu, X.K. Zhong, S.Y. Zhang, J. Appl. Electrochem. 40 (2010) 39–47.
[14] M. Yan, H.G. Ying, T.Y. Ma, Mater. Chem. Phys. 113 (2009) 764–767.
[15] H. Zhang, Y.W. Song, Z.L. Song, Mater. Corros. 59 (2008) 324–328.
[16] H.H. Man, H.C. Man, L.K. Leung, J. Magn. Magn. Mater. 152 (1996) 40–46.
[17] H.H. Man, H.C. Man, L.K. Leung, J. Magn. Magn. Mater. 152 (1996) 47–53.
[18] C.N. Cao, Principles of Electrochemistry of Corrosion, third ed., Chemical Industry Press, Beijing, 2008.
[19] H.L. Zeng, Z.D. Wu, J.W. Chen, P.R. Wu, Y.W. Qin, Manual of Electroplating Technology, second ed., China Machine Press, Beijing, 2003.
[20] B.M. Praveen, T.V. Venkatesha, Y. Arthoba Naik, K. Prashantha, Appl. Surf. Sci. 201 (2007) 5836–5842.
[21] B.M. Praveen, T.V. Venkatesha, Appl. Surf. Sci. 254 (2008) 2418–2424.
[22] A. Gomes, M.I. da Silva Pereira, M.H. Mendonca, F.M. Costa, J. Solid State Electrochem. 9 (2005) 190–196.
[23] Y. Zhou, H. Zhang, B. Qian, Appl. Surf. Sci. 253 (2007) 8335–8339.
[24] C.M. Bertelsen, F.J. Boerio, Prog. Org. Coat. 41 (2001) 239–246.
[25] C.N. Cao, J.Q. Zhang, An Introduction to Electrochemical Impedance Spectroscopy, first ed., Science Press, Beijing, 2002.
[26] D. Zhu, J. Wim, van Ooij, Corros. Sci. 45 (2003) 2177–2197.
[27] M.L. Zheludkevich, R. Serra, M.F. Montemor, I.M. Miranda Salvado, M.G.S. Ferreira, Surf. Coat. Technol. 200 (2006) 3084–3094.
[28] A. Cabral, R.G. Duarte, M.F. Montemor, M.L. Zheludkevich, M.G.S. Ferreira, Corros. Sci. 47 (2005) 869–881.
[29] M.G.S. Ferreira, R.G. Duarte, M.F. Montemor, A.M.P. Simões, Electrochim. Acta 49 (2004) 2927–2935.
[30] C. Khaldi, H. Mathlouthi, J. Lamloumi, J. Alloys Compd. 479 (2009) 284–289.
[31] W. Shang, B.Z. Chen, X.C. Shi, Y. Chen, X. Xiao, J. Alloys Compd. 474 (2009) 541–545.